

# Monte Carlo simulations of self-assembling hexagonal and cage-like bifunctional periodic mesoporous materials

Alessandro Patti,<sup>\*a</sup> Allan D. Mackie<sup>b</sup> and Flor R. Siperstein<sup>c</sup>

Received 20th July 2009, Accepted 24th August 2009

First published as an Advance Article on the web 16th September 2009

DOI: 10.1039/b914537k

Self-assembly of lyotropic liquid crystalline mesophases formed by amphiphilic molecules was studied using computer simulations. The addition of an inorganic and two hybrid organic–inorganic precursors, one with a bridging and the other with a terminal organic functionality, lead to the formation of bifunctional hexagonally-packed mesoporous materials. These structures exhibit very ordered and uniform mesopores with the organic functional groups located in the cylindrical pores and in their walls, and are found to be stable over a relatively broad range of precursor concentrations. Hexagonal-to-lamellar and hexagonal-to-cubic phase transitions have been observed at constant surfactant concentrations by tuning the relative content of the hybrid precursors which modify the overall solvophilic character of the solvent and, as a consequence, the surfactant solubility in its surrounding environment. The long range ordered cubic phases show interconnected, roughly spherical mesocages of uniform size and an interesting distribution of the organic functionalities.

## Introduction

Ordered mesoporous silica materials have captured the interest of the scientific community since the first synthesis performed by Beck and coworkers.<sup>1,2</sup> Their structural properties, such as large surface area and narrow pore size distribution, along with the broad range of possibilities to tune them by changing synthesis conditions, template, and/or (organo)silica precursors, have given an extraordinary impetus to further research in a large number of applications, such as separation,<sup>3</sup> catalysis,<sup>4</sup> drug delivery,<sup>5</sup> and sensor design.<sup>6</sup> In particular, a significant effort has been devoted to including functional groups into the pores,<sup>7–9</sup> pore walls,<sup>10–12</sup> and, more recently, into both.<sup>13,14</sup> The functionalization of porous materials has been achieved for powders (as in the references mentioned earlier), monoliths<sup>15</sup> and thin films.<sup>16,17</sup> The incorporation of bridging organosilica precursors (OSPs) of the form  $(R'O)_3\text{-Si-R-Si-(OR')}_3$  (where R and R' denote generic organic groups) into the silica framework gave rise to the discovery of periodic mesoporous organosilicas (PMOs).<sup>10–12</sup> This addition can significantly modify the dielectric constant of the material and improve its mechanical properties.<sup>18</sup> Nevertheless, even when the organic groups in the bridging position are accessible for reaction, they are not as reactive as the terminal organic group R in OSPs of the form  $(R'O)_3\text{-Si-R}$ , due to steric and electronic differences.<sup>11,12</sup> The simultaneous presence of OSPs containing terminal and bridging organic groups led to bifunctional periodic mesoporous organosilicas (BPMOs) with the functional groups at a nanoscale distance from each

other. These materials can be obtained by grafting the precursor with a terminal functionality into the pores of PMOs, or in one single step by co-condensation of two OSPs, being the most preferred way of synthesis.<sup>13,14,19–21</sup> BPMOs represented a step ahead in the family of functionalized mesoporous materials as they couple the higher reactivity of the organic terminal groups available in the pores, to the higher flexibility given by the bridging organic groups to the pore walls. As a result, the pore walls can better follow the curvature of the cylindrical aggregates, and the overall performance of the material during and after the template removal improves. This feature, as already discussed for PMOs,<sup>22</sup> can lead to a partial or even complete crystalline order of the pore walls, and hence can be a further improvement on catalysis and sorption/separation processes.

Hexagonally-packed BPMOs were first synthesized by Asefa *et al.* who performed co-condensation of a bridging OSP, bis-(triethoxysilyl)ethylene, with triethoxyvinylsilane as a terminal OSP, and cetyltrimethylammonium bromide (CTEABr) as the structure directing agent.<sup>13</sup> They also proposed the possibility of incorporating a higher number of OSPs, and presented a trifunctional mesoporous structure with one terminal (vinyl or methyl) and two bridging (ethylene and methylene) groups. Since then, researchers have focused on the incorporation of various OSPs in order to couple different chemical-physical properties together in one single material. Jaroniec and coworkers used large heterocyclic bridging and mercaptopropyl terminal groups for the adsorption and removal of mercury ions from water solutions;<sup>23</sup> Corriu and coworkers reported the synthesis of BPMOs with an antagonistic bridging acid and terminal basic OSPs for applications as semipermeable membranes,<sup>21</sup> and Zeidan *et al.* used bifunctional acid/basic mesoporous materials to mimic the catalytic behavior of enzymes;<sup>24</sup> Inagaki and coworkers obtained sulfuric acid-functionalized mesoporous benzene-silicas to be used as solid acid catalysts.<sup>25</sup> Bifunctional materials can also have advantages in the design of materials for controlled drug release.<sup>26</sup>

<sup>a</sup>Soft Condensed Matter, Debye Institute for Nanomaterials Science, Utrecht University, Princetonplein 5, Utrecht 3584 CC, The Netherlands. E-mail: a.patti@uu.nl

<sup>b</sup>Departament d'Enginyeria Química, Universitat Rovira i Virgili, Av. Països Catalans, 26, Tarragona 43007, Spain

<sup>c</sup>School of Chemical Engineering and Analytical Science, University of Manchester, Manchester M60 1QD, UK

Functionalization of mesoporous materials has been also extended to three-dimensional (3D) cubic mesophases, presenting pores of roughly spherical shape (also called *cages*), interconnected by narrow channels. It is generally accepted that such structures can represent a further improvement with respect to the 1D hexagonally-packed materials, because of their 3D porous network.<sup>27,29</sup> Their diameter is in the order 3–9 nm, whereas the linking channels (or windows) show a relevant range from few angstroms<sup>28</sup> up to several nanometres.<sup>29</sup> In the last fifteen years, self-assembling cage-type mesostructures of different symmetries have been synthesized<sup>30–32</sup> and become more and more attractive due to the possibility to perform a double tuning on the size of the cages and on that of the channels, and, hence, to better control the diffusion of guest molecules in targeted applications,<sup>32,33</sup> such as metal ion trapping<sup>34</sup> or adsorption.<sup>29</sup> Recently, Garcia-Bennet and coworkers prepared, under strong basic conditions (pH > 11), 3D cubic mesocaged materials with  $Pm\bar{3}n$  symmetry using CTEABr and two common silica precursors, tetraethyl orthosilicate (TEOS) and (3-aminopropyl)triethoxysilane (APES).<sup>35</sup> They performed several one-pot syntheses at different molar ratios of surfactant/APES and found a cubic structure when this ratio is 0.6. The main effect of APES in the mechanism proposed by these authors is based on the penetration of its solvophobic chain into the aggregates, rather than in the interactions that could be established between the charged ammonium ions and the surfactant headgroups, which instead, explains the formation of mesocages of face-centered cubic symmetry.<sup>36</sup> Among other functional groups, amines are of great interest for CO<sub>2</sub> capture and separation, and for removal of heavy ions from water solutions.<sup>38</sup> To this end, very ordered and stable amino-functionalized cubic SBA-1 mesoporous materials were obtained under acid conditions by co-condensation of CTEABr with TEOS and (3-aminopropyl)trimethoxysilane.<sup>37</sup>

To the best of our knowledge, the first attempt to synthesize bifunctional cage-like mesoporous materials was very recent.<sup>39</sup> By a one-pot synthesis with CTEABr, functionalized SBA-1 mesophases containing ethane bridging groups in the silica framework and terminal thiol groups in the pore channels were prepared. The resulting material revealed good adsorption properties for mercury ions and, hence, a potential role in soil and water remediation. Jaroniec and coworkers obtained mesoporous organosilicas by co-condensation of TEOS with two organosilica precursors containing bridging isocyanurate and ethane groups.<sup>27</sup> They tested a method for the template removal based on a short extraction and a soft heating under nitrogen. The characterization of the resulting material by different techniques showed that, although a significant shrinkage was detected, the order of the structure was preserved.

In this work, we performed Monte Carlo (MC) simulations to model the self-assembly of BPMOs obtained by co-condensation of two hybrid OSPs and a pure silica precursor. Our interest is mainly focused on the analysis of the hexagonally-packed and cage-like cubic structures and, in particular, on the distribution of the functional groups in their pores and pore walls. In addition, we analyze the transition from hexagonal to cubic cage-like phases which is deeply linked to the concentration of the hybrid organosilica precursors in the system.

## Model and simulation methodology

We studied the self-assembly of liquid crystalline mesophases using a coarse-grained lattice model, first applied by Larson *et al.* who investigated the aggregation behavior of amphiphilic monomers in systems containing water-like and oil-like solvents.<sup>40</sup> In this model, space is organized into a three dimensional cubic network of sites, which are all occupied by the solvent, precursors, or surfactant. As already explained in previous work,<sup>41–43</sup> the advantage of this model is that it permits a better appreciation of the ordered periodicity of the mesoporous structures obtained by reducing the many complex properties of the system to the most representative ones. Our system is composed of five components. Each component is modelled as a chain of connected sites (see Fig. 1): a surfactant, T<sub>5</sub>HH<sub>3</sub>, with a linear solvophobic tail of five segments *T*, and a solvophilic bulky head made up of four segments *H*; a pure silica precursor, I<sub>2</sub>; two OSPs, I<sub>2</sub>THT<sub>3</sub> and I<sub>2</sub>THTI<sub>2</sub>, with a terminal and a bridging organic functionality, respectively; and a solvent, S, which has not been modelled explicitly. Each segment occupies one single site of the lattice box, and hence no overlaps are allowed. From now on, the tail segments in between the beads *H* and *I* of the precursors, are called *T*<sub>α,t</sub> and *T*<sub>α,b</sub> if they belong to the terminal or bridging precursor, respectively.

The *T* (*H*) segments in the precursor chains are as solvophobic (solvophilic) as those of the surfactant, whereas the inorganic bead, *I*, which is soluble in the solvent, has a strong interaction with the surfactant heads. Each bead interacts with its nearest and diagonally-nearest neighbors. The total number of neighbors surrounding a given bead defines the coordination number of the cubic lattice, that is  $z = 26$ . The global interchange energy between a generic pair of sites *i* and *j* is defined as

$$\omega = \varepsilon_{ij} - (\varepsilon_{ii} + \varepsilon_{jj})/2 \quad (1)$$

with  $i \neq j$  and  $\varepsilon_{ij}$  the individual pair interactions. A detailed summary of the six independent interaction parameters is given in Table 1.

In order to displace the chains in the simulation box and hence make the system evolve from a completely random configuration to an ordered configuration, we performed Monte Carlo simulations in the *NVT* ensemble. An elongated box of volume

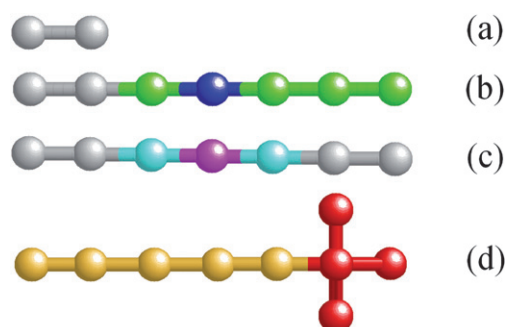


**Fig. 1** Modelled precursor and surfactant chains. (a) Pure silica precursor, I<sub>2</sub>; (b) OSP I<sub>2</sub>THT<sub>3</sub>; (c) OSP I<sub>2</sub>THTI<sub>2</sub>; (d) surfactant T<sub>5</sub>HH<sub>3</sub>. Surfactant heads and tails are shown in red and yellow, respectively; the inorganic beads in gray; *H* bead of I<sub>2</sub>THT<sub>3</sub> in blue; *H* bead of I<sub>2</sub>THTI<sub>2</sub> in magenta; *T* beads of I<sub>2</sub>THT<sub>3</sub> in green; *T* beads of I<sub>2</sub>THTI<sub>2</sub> in cyan.

**Table 1** Global interchange energies between the beads in the system. Note that  $\omega_{ij} = 0$  for definition

Pair of beads	H-T	H-I	H-S	T-I	T-S	I-S
$\omega_{ij}$	1	-2	0	1	1	0

$24 \times 24 \times 100$  was used to study the phase separation between a hybrid-rich phase and a solvent-rich phase; whereas a cubic box of volume  $40^3$  was used to analyze the structural properties of the resulting ordered mesophases. In both cases, periodic boundary conditions were applied. All the chains have been displaced by configurational bias moves (partial and complete regrowth).<sup>44</sup> The linear precursor chains were also moved by reptation, according to the Metropolis algorithm. The dimensionless temperature reads  $T^* = k_B T / \omega_{HT}$ , where  $k_B$  is the Boltzmann constant,  $T$  the absolute temperature, and  $\omega_{HT}$  is the surfactant head–tail interaction energy. All the simulations have been run at  $T^* = 8.0$ .

To check the distribution of the hybrid precursors in the silica framework, we calculated the composition profiles  $\rho_i(r)$  of the sites  $i$  at radial distance  $r$  from the center of mass in spherical aggregates, or from the line connecting the center of mass of quasi-circular cross-sections in cylindrical aggregates. We assume that two surfactant chains belong to the same aggregate if they share at least one of their tail beads as a neighbor (see ref. 41 for more details). Since the volume fraction of the precursors can be much smaller than that of the surfactant, we prefer to normalize the density profiles dividing  $\rho_i(r)$  by the global density  $\rho_{i,0}$ . Therefore,  $\rho_{i,N}(r) \equiv \rho_i(r) / \rho_{i,0}$  should converge to 1 at large radial distances  $r$ .

## Results

In this section, we first report on the phase behavior of the present system and then on the main structural features of the mesophases observed. To locate the range of stability of the ordered mesophases, we took as a reference the phase diagram of the four-component system (4CS)  $T_5HH_3/I_2/I_2THT_3/S$ , already studied in a previous work.<sup>45</sup> The different nature of the two OSPs makes the phase behavior of the five-component system (5CS) significantly more complex than that of the 4CS. Phase segregation is observed in both OSPs due to the presence of a double inorganic terminal group,  $-I_2$ , which forms very strong attractions with the surfactant heads. Additionally, the precursor  $I_2THTI_2$  is highly compatible with the solvent and the pure inorganic precursor, increasing the solubility of the surfactant in the solution. In other words,  $I_2THTI_2$  behaves like a *cosolvent*. In contrast, the strong solvophobic terminal group  $-T_3$  reduces the solubility of the surfactant in the solution. For this reason,  $I_2THT_3$  can be considered as a *cosurfactant*. The behavior of cosurfactants and cosolvents in simple systems has been described by Chennamsetty *et al.*<sup>46</sup> In the systems studied, when both OSPs are present, the resulting effect on the solubility of the surfactant is a compromise between these antagonistic behaviors. We observed that by keeping the concentration of  $I_2THTI_2$  below 20% by volume, the 5CS self-assembles into a hexagonally packed phase generally at equilibrium with a very dilute solvent-

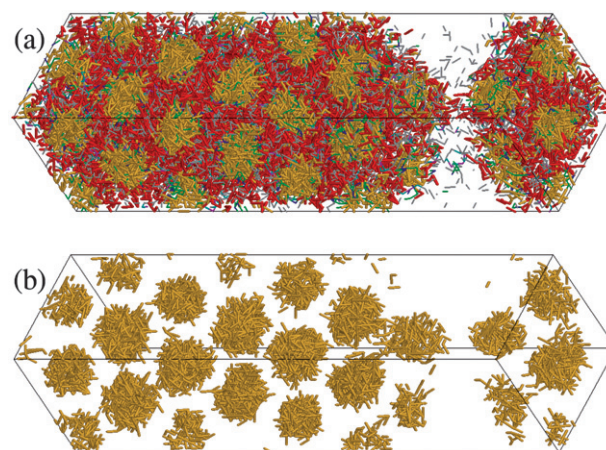


**Fig. 2** Hexagonally-packed phase at equilibrium with a solvent-rich phase observed at  $T^* = 8.0$  in a lattice box of volume  $24 \times 24 \times 100$ . Global concentrations: 40%  $T_5HH_3$  – 10%  $I_2$  – 10%  $I_2THT_3$  – 4%  $I_2THTI_2$ . The solvent is not shown. Only the surfactant tails are shown in (b) to appreciate the hexagonal order. See caption of Fig. 1 for colors.

rich phase. A typical case of phase separation with formation of a dense ordered phase is shown in Fig. 2.

In our simple model, two main effects can be identified as those driving the separation between dilute and concentrated phases: (i) the significant  $I$ – $H$  attraction between the inorganic beads of both precursors and the surfactant solvophilic heads, and (ii) the  $T$ – $S$  repulsion between the surfactant solvophobic tails and the solvent (see Table 1). The combination of both effects leads to a denser phase where the higher surfactant concentration along with the interactions established between the beads, sparks the self-assembly process.

It was observed in experiments that amphiphilic systems containing TEOS and the hybrid precursor phenyl-3-aminopropyltrimethoxysilane (PAP) exhibit a hexagonal-to-lamellar transition at high PAP concentrations.<sup>47</sup> This result, which has been also confirmed in our previous simulations on 4CSs by modelling PAP with  $I_2THT_3$ ,<sup>45</sup> was attributed to the strong solvophobic character of the OSP, which provokes the swelling of the core in the cylindrical aggregates and hence the formation of the lamellar order. In 5CSs, we still detect hexagonally ordered structures over a broad range of concentrations. However, if the volume fraction of  $I_2THTI_2$  or  $I_2THT_3$  becomes very high, the distinctive nature of the two OSPs emerges and affects the structure of the phases at equilibrium. In particular, we noticed a transition from a hexagonal to a cubic phase by increasing the concentration of the bridging OSP above 20% and decreasing that of the terminal OSP below 10%. *Vice versa*, if the concentration of the bridging precursor gradually fades out to zero, a hexagonal-to-lamellar transition is observed at  $I_2THT_3$  concentrations above  $\sim 20\%$ . The range of concentrations of the two OSPs which give cubic, hexagonal, or lamellar order is reported in Table 2.

In Fig. 3, we schematically locate the range of global OSP concentrations giving cubic, hexagonal, or lamellar structures, at constant concentrations of  $T_5HH_3$  (40%) and  $I_2$  (10%). The empty area is a high density region that we did not explore as the probability to displace chains and beads in a system containing

**Table 2** Global concentrations of  $I_2THTI_2$  and  $I_2THT_3$  in systems containing 40%  $T_5HH_3$  and 10%  $I_2$ , and resulting concentrations in the liquid crystal phase and in the dilute phase (if any). HEX: hexagonal, CUB: cubic, LAM: lamellar

Global concentrations (%)		Concentrations in surfactant-rich phase (%)					Concentrations in solvent-rich phase (%)			
$I_2THTI_2$	$I_2THT_3$	$T_5HH_3$	$I_2$	$I_2THTI_2$	$I_2THT_3$	Order	$T_5HH_3$	$I_2$	$I_2THTI_2$	$I_2THT_3$
0.0	10.0	54.9	13.0	0.0	13.3	HEX	0.2	2.6	0.0	0.2
0.0	15.0	50.9	11.9	0.0	19.1	HEX	0.5	3.0	0.0	0.4
0.0	18.0	50.3	11.7	0.0	23.0	LAM	0.8	3.0	0.0	0.6
0.0	20.0	49.2	11.4	0.0	23.5	LAM	0.8	3.7	0.0	0.5
0.0	25.0	46.0	10.8	0.0	28.3	LAM	1.2	4.2	0.0	1.0
2.0	20.0	46.0	10.9	2.2	23.1	LAM	1.3	3.4	0.5	0.7
2.0	30.0	40.0	10.0	3.0	20.0	LAM	One phase			
4.0	10.0	52.1	12.2	5.2	12.5	HEX	0.3	3.2	0.4	0.3
5.0	15.0	47.3	11.1	5.6	17.6	HEX	0.0	3.8	1.1	0.4
5.0	20.0	40.0	10.0	5.0	20.0	HEX	One phase			
5.0	30.0	40.0	10.0	5.0	30.0	LAM	One phase			
7.0	7.0	51.6	12.0	8.5	9.0	HEX	1.0	3.6	1.1	0.3
10.0	0.0	56.5	12.9	13.1	0.0	HEX	0.8	3.5	2.0	0.0
10.0	4.0	52.6	12.0	12.2	5.1	HEX	0.7	3.8	2.4	0.2
10.0	20.0	40.0	10.0	10.0	20.0	HEX	One phase			
15.0	0.0	52.1	11.8	17.4	0.0	HEX	0.2	3.5	4.3	0.0
15.0	5.0	47.3	10.7	17.0	6.4	HEX	0.9	4.4	4.8	0.1
15.0	20.0	40.0	10.0	15.0	20.0	HEX	One phase			
20.0	0.0	40.0	10.0	20.0	0.0	CUB	One phase			
20.0	5.0	40.0	10.0	20.0	5.0	CUB	One phase			
20.0	10.0	40.0	10.0	20.0	10.0	HEX	One phase			
20.0	15.0	40.0	10.0	20.0	15.0	HEX	One phase			
25.0	5.0	40.0	10.0	25.0	5.0	CUB	One phase			
30.0	0.0	40.0	10.0	30.0	0.0	CUB	One phase			
30.0	5.0	40.0	10.0	35.0	5.0	CUB	One phase			

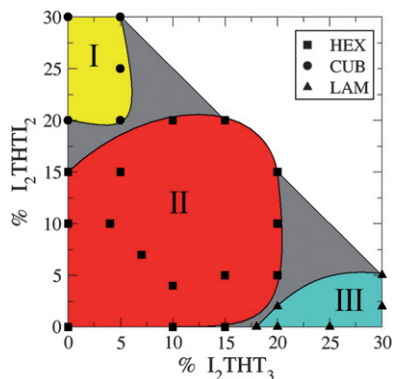


**Fig. 3** Global concentrations (solid symbols) of terminal and bridging OSPs which give cubic (I), hexagonal (II), or lamellar (III) ordered structures, at 40%  $T_5HH_3$  and 10%  $I_2$ . The areas in grey indicate regions of transition from a liquid crystal phase to another. Systems containing less than 15% of solvent have not been studied.

less than 15% of solvent, would be extremely low. Systems containing an extremely low solvent concentration are more efficiently modelled using approaches accepted for simulating polymer melts, such as the bond fluctuating model for lattice simulations<sup>48</sup> or dissipative particle dynamics for off lattice simulations.<sup>49</sup> The grey-shaded areas denote those regions of transition where there is no evidence of a clear and unique cubic, hexagonal, or lamellar order, and should be investigated in future work. Over a quite broad range of concentrations, the system self-assembles in hexagonally-packed liquid crystals (area II), whereas cubic (I) or lamellar (III) order is only observed at

high concentrations of one of the OSPs. The self-assembly in ordered structures can proceed *via* a phase separation between a dense and a dilute phase at low-to-moderate precursor concentrations; otherwise, only one phase is observed. In Fig. 4, we show two equilibrium configurations of lamellar (a) and cubic mesophases (b). In Fig. 4b and 4d, we have displayed only the surfactant tails without the solvophilic coronas and the surrounding precursors to give clear evidence of the structural order.

The hexagonal-to-lamellar and hexagonal-to-cubic phase transitions are the result of the increasing concentration of the cosurfactant  $I_2THT_3$  and cosolvent  $I_2THTI_2$ , respectively. When the amount of the cosurfactant increases, the system needs to pack the total amphiphilic moiety ( $T_5HH_3$  plus  $I_2THT_3$ ) more efficiently, in order to minimize the extent of mixing between the solvent and the solvophobic tails ( $-T_5$  group of the surfactant and  $-T_3$  group of the cosurfactant). This is achieved by arranging the amphiphilic chains in stacks of smectic layers whose packing results to be higher than in hexagonal or cubic liquid crystals. Hexagonal-to-lamellar transitions induced by a cosurfactant have been also observed experimentally.<sup>50</sup> On the other hand, decreasing the concentration of the cosurfactant to zero and increasing that of the cosolvent have a diluting effect on the aggregates, make them less packed, and favor high surface curvatures.<sup>51</sup>

In Fig. 5 and 6, the normalized density profiles of the organic functional groups of  $I_2THT_3$  and  $I_2THTI_2$ , respectively, are given. To better analyze their distribution with respect to the inorganic framework, we have included in both figures the density profile of the inorganic beads,  $I$ , of the pure silica and organosilica precursors as a whole. The total amount of  $I$  beads

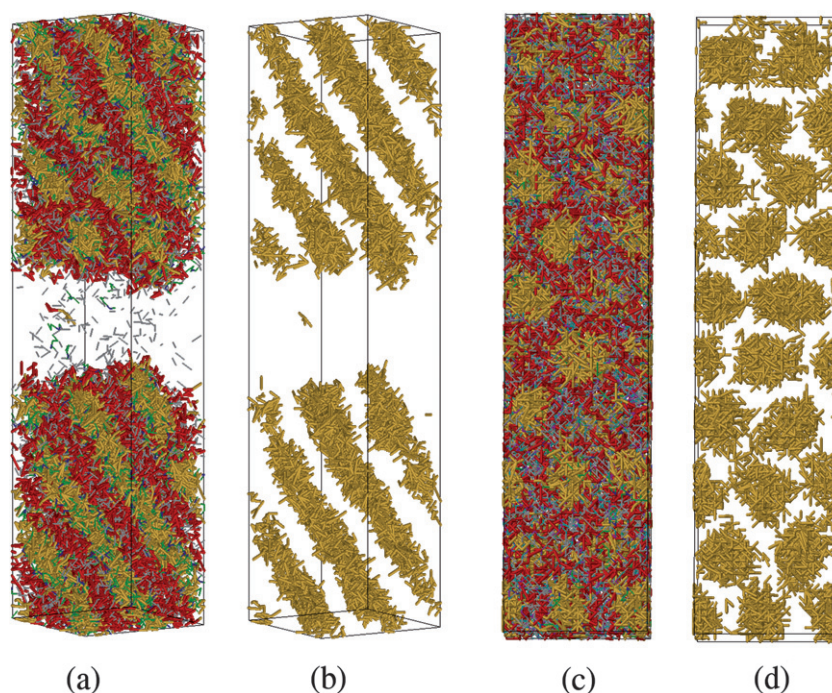


**Fig. 4** (a,b) Lamellar phase at equilibrium with a dilute phase observed in the system 40%  $T_5HH_3$ , 10%  $I_2$ , and 18%  $I_2THT_3$ . (c,d) Cage-like cubic structure obtained in the system 40%  $T_5HH_3$ , 10%  $I_2$ , 20%  $I_2THTI_2$ , and 5%  $I_2THT_3$ . The solvent is not shown. In figures (b) and (d), only the surfactant tails are shown to appreciate the structural order. See caption of Fig. 1 for colors.

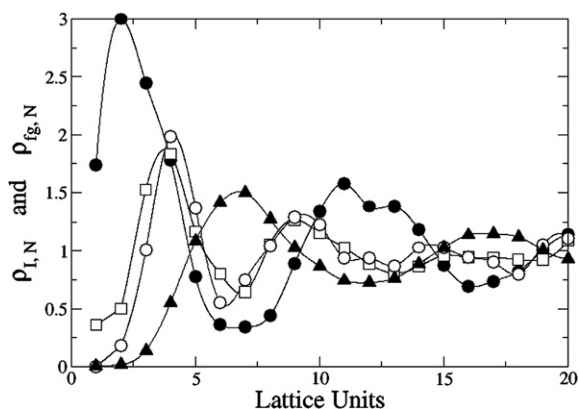


**Fig. 5** Normalized distribution profiles of the functional group ( $fg$ ) of  $I_2THT_3$  across a cylindrical micelle in systems containing 51.8%  $T_5HH_3$ , 11.8%  $I_2$ , 5.1%  $I_2THT_3$  and 12.1%  $I_2THTI_2$ . Symbols:  $T_{\alpha,t}$  ( $\square$ ),  $T_{terminal}$  ( $\bullet$ ),  $H$  ( $\circ$ ). The symbols ( $\blacktriangle$ ) refer to the overall normalized distribution of the inorganic moiety,  $I$ , belonging to all precursors.

constitutes the silica framework surrounding the aggregates, and therefore it is important to identify the location of the different functional groups with respect to it. Each of the three distribution profiles of the organic beads belonging to  $I_2THT_3$  reveal very well defined peaks, being clearly separated from that of the inorganic moiety surrounding the pore (solid triangles in Fig. 5). This is especially evident for the terminal solvophobic group,  $-T_3$ , being almost completely accumulated inside the core of the cylindrical aggregate and absent in the corona that will constitute the pore walls once the material is formed. As far as the  $T_{\alpha,t}$  and  $H$  groups are concerned, their highest

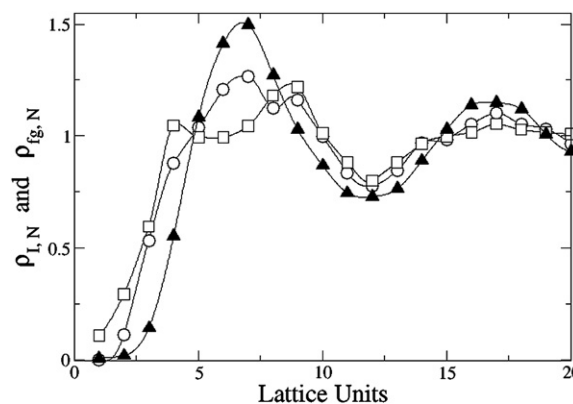


**Fig. 6** Normalized distribution profiles of beads belonging to  $I_2THTI_2$  across a cylindrical micelle in systems containing 51.8%  $T_5HH_3$ , 11.8%  $I_2$ , 5.1%  $I_2THT_3$  and 12.1%  $I_2THTI_2$ . Symbols:  $T_{\alpha,b}$  ( $\square$ ),  $H$  ( $\circ$ ). The symbols ( $\blacktriangle$ ) refer to the overall normalized distribution of the inorganic moiety,  $I$ , belonging to all precursors.

concentration is detected at the surface of the cylindrical core, where it creates a sort of intermediate layer between the pore surface and the  $-T_3$  groups. A similar result was formerly obtained in systems containing only one hybrid precursor,  $I_2THT_3$ ,<sup>45</sup> although here the penetration of the terminal  $-T_3$  groups into the core is slightly deeper, most probably because of the better solvent quality and the higher surfactant solubility due to the presence of  $I_2THTI_2$ . Nevertheless, we can safely say that the distribution profile of the functional group  $-THT_3$  in hexagonally-packed structures is not significantly affected by the presence of a bridging OSP.

By contrast, Fig. 6 brings to light a very deep interconnection between the organic bridging functional group of  $I_2THTI_2$  and the inorganic framework, as confirmed by the quasi-overlap of the corresponding density profiles. The split detected in the peak of the  $T_{\alpha,b}$  profile arises from the intrinsic symmetric architecture of the bridging precursor, and creates a sort of protecting covering around the solvophilic functional bead  $H$ . This covering could represent a critical barrier in the case where the solvophilic functional group has to be an active site for a given application, as its availability would be definitely more limited.

When we increase the concentration of  $I_2THTI_2$  and decrease that of  $I_2THT_3$ , the 5CS experiences a hexagonal-to-cubic phase transition. The cubic phase is characterized by the presence of (roughly) spherical aggregates whose size distribution is relatively narrow and peaks at approximately 60 chains, as showed in Fig. 7. The smaller peaks, located at  $N \sim 120$ , 180, and 240, do not indicate the presence of elongated micelles, but rather the probability of two, three, or four solvophobic cores touching each other. Due to the high density in our system, this transitory event can be easily detected, especially for pairs of aggregates (see Fig. 8 (b)), but also for triplets or quadruplets. In the inset of Fig. 7, we show the three principal radii of gyration of the clusters, which are in between 2 and 3 lattice units for the most probable sizes. The similarity between the three radii of gyration confirms the presence of spherical aggregates.

A clear representation of the cage-to-cage interconnection is shown in Fig. 9, where four spherical aggregates, isolated from

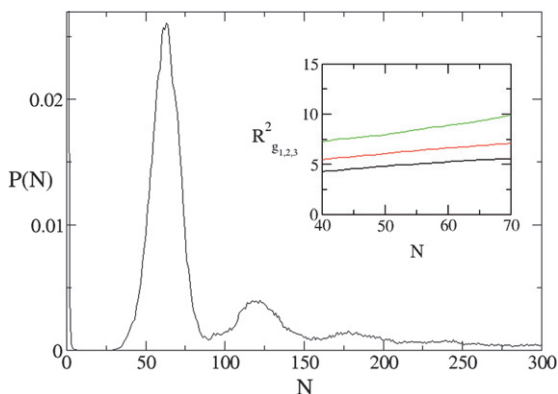


**Fig. 7** Cluster size distribution and (inset) principal radii of gyration of a system containing 40%  $T_5HH_3$ , 10%  $I_2$ , 20%  $I_2THTI_2$ , 5%  $I_2THT_3$  and 25% solvent.

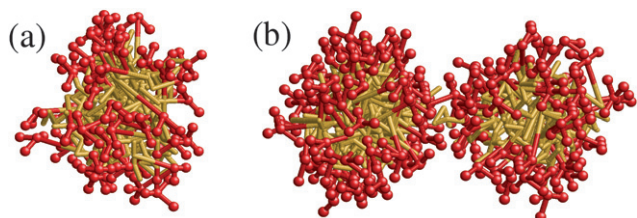


**Fig. 8** (a, b) Spherical aggregates observed in a system containing 40%  $T_5HH_3$ , 10%  $I_2$ , 30%  $I_2THTI_2$ , and 20% solvent. No OSP with a terminal organic group is present. In (b) two aggregates are touching each other. The tails and heads are in yellow and red, respectively.

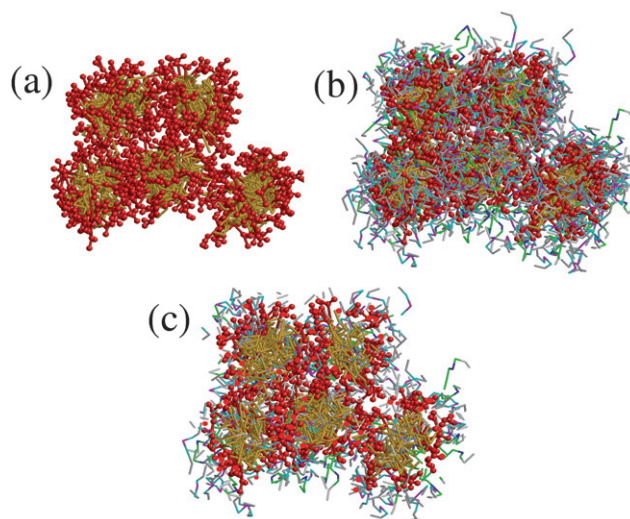


**Fig. 9** Snapshot of five interconnected mesocages observed in the system containing 40%  $T_5HH_3$ , 10%  $I_2$ , 20%  $I_2THTI_2$ , 5%  $I_2THT_3$  and 15% solvent. (a) Template only. (b) Inorganic and hybrid precursors covering the template. (c) Cross section of the aggregate, indicating the presence of well defined spherical solvophobic cores. See caption of Fig. 1 for colors.

the bulk phase, result to be linked by small *bottlenecks*. Their opening depends on the distance between the cages, or, equivalently, on the surfactant concentration in the system. Although we did not take into account here the effect of the surfactant architecture on the structural properties of the ordered phases, we expect that both the shape and size of the surfactant head would play an important role in determining the diameter of linking channels. At low surfactant concentrations, the aggregates would be completely separated by the inorganic wall and no interconnecting channels would be observed. However, a long linear headgroup could balance this effect.

If we look at the density distribution profiles of Fig. 10, we see that most of the inorganic layer is located around the corona of

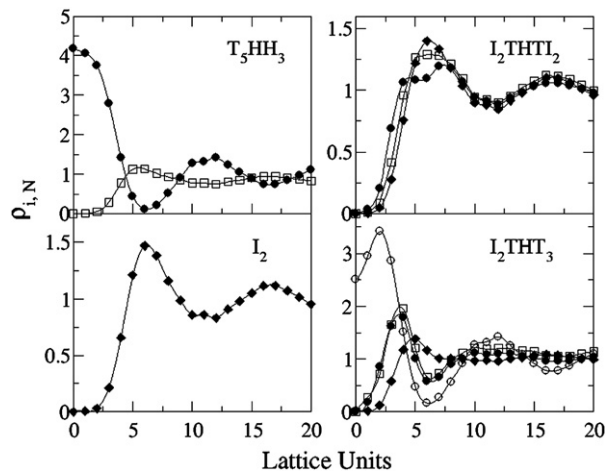


**Fig. 10** Normalized density profiles observed in a spherical aggregate with 60 surfactant chains. The squares, diamonds, solid and empty circles represent  $H$ ,  $I$ ,  $T$  (or  $T_{\alpha}$ ), and  $T_{terminal}$  beads, respectively. Concentrations: 40%  $T_5HH_3$ , 10%  $I_2$ , 20%  $I_2THTI_2$ , 5%  $I_2THT_3$  and 15% solvent.

the aggregates, where the concentration of the surfactant heads shows a peak as well. The pure silica and hybrid precursors do not exhibit a density peak separating the coronas of neighboring aggregates, but, instead, they organize around them, and, once the template has been removed, form interconnecting channels. As also observed for hexagonally-packed phases, the terminal solvophobic group of I<sub>2</sub>THT<sub>3</sub> penetrates deeply inside the core of the cage, whereas the other functional groups are most likely distributed around or into the solvophilic corona. For cubic mesophases not containing a terminal OSP, the density distribution of the surfactant and precursors do not show significant differences from those in Fig. 10, and are not shown here.

## Conclusions

We performed computer simulations to study the phase behavior and the self-assembly of systems composed of an amphiphilic template, a pure silica precursor, two organosilica precursors with terminal or bridging functionalities, and a solvent. By using a simple coarse-grained model, we showed that these systems are able to form bifunctional ordered mesophases, such as lamellar, cage-like cubic, or hexagonally-packed cylindrical structures. By tuning the concentrations of the two hybrid organosilica precursors, which have opposite effects on the solubility of the surfactant, hexagonal-to-lamellar or hexagonal-to-cubic phase transitions are observed. In particular, by increasing the concentration of the bridging precursor, which behaves as a cosolvent, we favor the formation of the cubic phase, whereas a high concentration of the terminal precursor, which can be considered as a cosurfactant, leads the system to form lamellar phases. Removing the template from the hexagonally-packed or cubic phases leads to the formation of mesoporous structures containing functional organic groups in the silica framework and in the pores. The distribution of these groups has been discussed in terms of composition profiles, and the possibility to use them as active sites for selective operations has been analyzed. The transition from hexagonal to cubic phases gives rise to the formation of interconnected spherical cavities (or cages). Networks of 3D quasi-cylindrical pores with periodical bottlenecks located at the intersection of neighboring cages have been observed and the composition profiles of the functional groups into the pores and into the pore walls, result to be basically identical to those observed for the cylindrical aggregates.

Although the terminal OSP penetrates the core of the aggregate and the bridging OSP remains in the corona of the aggregate, no microphase segregation was observed between the OPS in the axial direction of the cylindrical micelles. In the systems containing cubic structures, the distribution of OSPs was observed in the radial direction, but no evident segregation was observed in the regions of the windows between cages and the cage walls.

## Acknowledgements

AP gratefully acknowledges a postdoctoral fellowship from Utrecht University. ADM acknowledges the Ministerio de Ciencia e Innovación, project no. CTQ2008-06469/PPQ. FRS acknowledges funding from DeSANNs EC, project no. SES6-CT-2005-020133.

## References

- 1 J. S. Beck, J. C. Vartuli, W. J. Roth, M. E. Leonowicz, C. T. Kresge, K. D. Schmitt, C. T. W. Chu, D. H. Olson, E. W. Sheppard, S. B. Mccullen, J. B. Higgins and J. L. Schlenker, *J. Am. Chem. Soc.*, 1992, **114**, 10834.
- 2 C. T. Kresge, M. E. Leonowicz, W. J. Roth, J. C. Vartuli and J. S. Beck, *Nature*, 1992, **359**, 710.
- 3 H. Yoshitake, T. Yokoi and T. Tatsumi, *Chem. Mater.*, 2003, **15**, 1713; S. Dai, M. C. Burleigh, Y. Shin, C. C. Morrow, C. E. Barnes and Z. Xue, *Angew. Chem., Int. Ed.*, 1999, **38**, 1235; K. Z. Hossain and L. Mercier, *Adv. Mater.*, 2002, **14**, 1053.
- 4 J. d. A. A. Soler-Illia Galo, C. Sanchez, B. Lebeau and J. Patarin, *Chem. Rev.*, 2002, **102**, 4093; M. E. Davis, *Nature*, 2002, **417**, 813; A. Corma, *Chem. Rev.*, 1997, **97**, 2373; A. Sayari, *Chem. Mater.*, 1996, **8**, 1840.
- 5 M. Vallet-Regí, F. Balas and D. Arcos, *Angew. Chem., Int. Ed.*, 2007, **46**, 7548; C.-Y. Lai, B. G. Trewyn, D. M. Jeftinija, K. Jeftinija, S. Xu, S. Jeftinija and V. S. Y. Lin, *J. Am. Chem. Soc.*, 2003, **125**, 4451.
- 6 V. S. Y. Lin, C.-Y. Lai, J. Huang, S.-A. Song and S. Xu, *J. Am. Chem. Soc.*, 2001, **123**, 11510; M. C. Burleigh, S. Dai, E. W. Hagaman and J. S. Lin, *Chem. Mater.*, 2001, **13**, 2537.
- 7 M. H. Lim, C. F. Blanford and A. Stein, *J. Am. Chem. Soc.*, 1997, **119**, 4090.
- 8 L. Mercier and T. J. Pinnavaia, *Adv. Mater.*, 1997, **9**, 500.
- 9 X. Feng, G. E. Fryxell, L.-Q. Wang, A. Y. Kim, J. Liu and K. M. Kemner, *Science*, 1997, **276**, 923.
- 10 T. Asefa, M. J. MacLachan, N. Coombs and G. A. Ozin, *Nature*, 1999, **402**, 867.
- 11 S. Inagaki, S. Guan, Y. Fukushima, T. Ohsuna and O. Terasaki, *J. Am. Chem. Soc.*, 1999, **121**, 9611.
- 12 B. J. Melde, B. T. Holland, C. F. Blanford and A. Stein, *Chem. Mater.*, 1999, **11**, 3302.
- 13 T. Asefa, M. Kruk, M. J. MacLachlan, N. Coombs, H. Grondey, M. Jaroniec and G. A. Ozin, *J. Am. Chem. Soc.*, 2001, **123**, 8520.
- 14 E. Besson, A. Mehdi, V. Matsuura, Y. Guari, C. Reye and R. J. P. Corriu, *Chem. Commun.*, 2005, 1775.
- 15 S. S. Park and C. S. Ha, *Chem. Rec.*, 2006, **6**, 32.
- 16 G. J. A. A. Soler-Illia and P. Innocenzi, *Chem.-Eur. J.*, 2006, **12**, 4478.
- 17 C. Sanchez, C. Boissiere, D. Grosso, C. Laberty and L. Nicole, *Chem. Mater.*, 2008, **20**, 682.
- 18 Y. F. Lu, H. Y. Fan, N. Doke, D. A. Loy, R. A. Assink, D. A. LaVan and C. J. Brinker, *J. Am. Chem. Soc.*, 2000, **122**, 5258.
- 19 M. C. Burleigh, M. A. Markowitz, M. S. Spector and B. P. Gaber, *Chem. Mater.*, 2001, **13**, 4760.
- 20 M. C. Burleigh, M. A. Markowitz, M. S. Spector and B. P. Gaber, *J. Phys. Chem. B*, 2001, **105**, 9935.
- 21 J. Alauzun, A. Mehdi, C. Reye and R. J. P. Corriu, *J. Am. Chem. Soc.*, 2006, **128**, 8718.
- 22 S. Inagaki, S. Guan, T. Ohsuna and O. Terasaki, *Nature*, 2002, **416**, 304.
- 23 O. Olkhoviy, S. Pikus and M. Jaroniec, *J. Mater. Chem.*, 2005, **15**, 1517.
- 24 R. K. Zeidan, S.-J. Hwang and M. E. Davis, *Angew. Chem., Int. Ed.*, 2006, **45**, 6332.
- 25 Q. H. Yang, M. P. Kapoor and S. Inagaki, *J. Am. Chem. Soc.*, 2002, **124**, 9694.
- 26 T. Asefa, A. N. Otuonye, G. Wang, E. A. Blair, R. Vathyam and K. Denton, *Adsorption*, 2009, **15**, 287.
- 27 R. M. Grudzien, J. P. Blizt, S. Pikus and M. Jaroniec, *Microporous Mesoporous Mater.*, 2009, **118**, 68.
- 28 T.-W. Kim, R. Ryoo, M. Kruk, K. P. Gierszal, M. Jaroniec, S. Kamiya and O. Terasaki, *J. Phys. Chem. B*, 2004, **108**, 11480.
- 29 J. Fan, C. Yu, F. Gao, J. Lei, B. Tian, L. Wang, Q. Luo, B. Tu, W. Zhou and D. Zhao, *Angew. Chem., Int. Ed.*, 2003, **42**, 3146.
- 30 Q. Huo, D. I. Margolese, U. Ciesla, P. Feng, T. E. Gier, P. Sieger, R. Leon, P. M. Petroff, F. Schüth and G. D. Stucky, *Nature*, 1994, **368**, 317.
- 31 C. Yu, Y. Yua and D. Zhao, *Chem. Commun.*, 2000, 575.
- 32 A. E. Garcia-Bennett, K. Miyasaka, O. Terasaki and S. N. Che, *Chem. Mater.*, 2004, **16**, 3597.
- 33 C. Zapilko, Y. Liang and R. Anwender, *Chem. Mater.*, 2007, **19**, 3171.
- 34 S. A. El-Safty, A. A. Ismail, H. Matsunaga, H. Nanjo and F. Mizukami, *J. Phys. Chem. C*, 2008, **112**, 4825.

- 
- 35 R. Atluri, Y. Sakamoto and A. E. Garcia-Bennett, *Langmuir*, 2009, **25**, 3189.
- 36 S. N. Che, A. E. Garcia-Bennett, T. Yokoi, K. Sakamoto, H. Kunieda, O. Terasaki and T. Tatsumi, *Nat. Mater.*, 2003, **2**, 801.
- 37 H. Kao, C. Liao, A. Palani and Y. Liao, *Microporous Mesoporous Mater.*, 2008, **113**, 212.
- 38 J. Alauzun, E. Besson, A. Mehdi, C. Reye and R. J. P. Corriu, *Chem. Mater.*, 2008, **20**, 503.
- 39 H. Wu, C. Liao, Y. Pan, C. Yeh and H. Kao, *Microporous Mesoporous Mater.*, 2009, **119**, 109.
- 40 R. G. Larson, L. E. Scriven and H. T. Davis, *J. Chem. Phys.*, 1985, **83**, 2411.
- 41 A. Patti, A. D. Mackie and F. R. Siperstein, *Langmuir*, 2007, **23**, 6771.
- 42 A. Patti, F. R. Siperstein and A. D. Mackie, *J. Phys. Chem. C*, 2007, **111**, 16035.
- 43 F. R. Siperstein and K. E. Gubbins, *Langmuir*, 2003, **19**, 2049.
- 44 D. Frenkel and B. Smit, *Understanding Molecular Simulations: From Algorithms to Applications*, 2<sup>nd</sup> edn, Academic Press, San Diego, 2001.
- 45 A. Patti, A. D. Mackie, V. Zelenak and F. R. Siperstein, *J. Mater. Chem.*, 2009, **19**, 724.
- 46 N. Chennamsetty, H. Bock, L. F. Scanu, F. R. Siperstein and K. E. Gubbins, *J. Chem. Phys.*, 2005, **122**, 094710.
- 47 V. Zelenak, M. Badanicova, N. Murafa, and U. Vannio, unpublished work.
- 48 I. Carmesin and K. Kremer, *Macromolecules*, 1988, **21**, 2819.
- 49 R. D. Groot and P. B. Warren, *J. Chem. Phys.*, 1997, **107**, 4423.
- 50 F. Kleitz, J. Blanchard, B. Zibrowius and F. Schüth, *Langmuir*, 2002, **18**, 4963.
- 51 S. Liu, P. Cool, O. Collart, P. Van Der Voort, E. F. Vansant, O. I. Lebedev, G. Van Tendeloo and M. Jiang, *J. Phys. Chem. B*, 2003, **107**, 10405.